

Protein-like dynamical transition of hydrated polymer chains

L. Tavagnacco,¹ M. Zanatta,² E. Buratti,¹ B. Rosi,³ B. Frick,⁴ F. Natali,⁵ J. Ollivier,⁴ E. Chiessi,⁶ M. Bertoldo,^{7,8} E. Zaccarelli,^{1,*} and A. Orecchini^{3,9,†}

¹*CNR-ISC and Department of Physics, Sapienza University of Rome, I-00185 Roma, Italy*

²*Department of Physics, University of Trento, I-38123 Trento, Italy*

³*Department of Physics and Geology, University of Perugia, I-06123, Perugia, Italy*

⁴*Institut Laue Langevin, F-38042 Grenoble, France*

⁵*CNR-IOM, Operative Group Grenoble (OGG), Institut Laue Langevin, F-38042 Grenoble, France*

⁶*Department of Chemical Science and Technologies,
University of Rome Tor Vergata, I-00133 Roma, Italy*

⁷*Department of Chemical and Pharmaceutical Sciences, University of Ferrara, I-44121 Ferrara, Italy*

⁸*CNR-ISOF, I-40129 Bologna, Italy*

⁹*CNR-IOM c/o Department of Physics and Geology, University of Perugia, I-06123, Perugia, Italy*

(Dated: June 18, 2022)

Combining elastic incoherent neutron scattering experiments at different resolutions and molecular dynamics simulations, we report the observation of a protein-like dynamical transition in Poly(N-isopropylacrylamide) chains. We identify the onset of the transition at a temperature T_d of about 225 K. Thanks to a novel global fit procedure, we find quantitative agreement between measured and calculated polymer mean-squared displacements at all temperatures and time resolutions. Our results confirm the generality of the dynamical transition in macromolecular systems in aqueous environments, independently of the internal polymer topology.

A long-debated phenomenon in the (bio)physical community is the occurrence of a dynamical transition in proteins, either globular or intrinsically disordered, that has been widely investigated by means of neutron scattering experiments [1]. As its name suggests, such a transition appears as a change of the protein dynamical properties, namely a steep increase of their atomic mobility, that is accompanied by the onset of anharmonic motions, at a specific dynamical transition temperature T_d . Concomitantly, the atomic motions that are specifically responsible for protein biological function at physiological temperatures become active [2, 3]. Much of the debate has been focused on the role played by water in the transition with several works supporting a water-induced scenario [4–8], but also with recent findings of a dynamical transition in dry protein powders [9]. Another direction of investigation concerns the generality of the phenomenon, that was found to occur in different bio-macromolecules, including DNA [10], RNA [11] and lipid bilayers [12]. Along this line, recent works [13, 14] reported evidence of a dynamical transition in concentrated Poly(N-isopropylacrylamide), PNIPAM, microgel suspensions, extending the realm of the dynamical transition to non-biological systems. Microgels are colloidal-scale particles made by covalently cross-linked polymer networks [15], that were shown to avoid water crystallization at low temperatures even in highly hydrated samples, i.e. down to a polymer weight fraction of ~ 43 wt% [13]. For these systems, a clear increase of the experimental mean-squared displacement (MSD) of the polymer atoms was observed, whereas atomistic

molecular dynamics simulations highlighted the pivotal role of water in the transition [14].

In the biophysical context, a dynamical transition was observed for structured proteins and also for their building blocks, namely polypeptides [16] and even amino acids [17]. Following a similar direction, it is now legitimate to ask whether the polymeric architecture has any influence on the occurrence of such a transition by examining the case of PNIPAM linear (non cross-linked) polymer chains. This polymer is mostly exploited for its thermoresponsive properties [18–20]: above room temperature, PNIPAM chains undergo a reversible coil-to-globule transition with increasing temperature T , which makes them suitable to mimic protein folding and to investigate protein cold denaturation [21]. The similarity of PNIPAM with proteins can be traced back to the amphiphilic character and the associated complex energy landscape, endowed with multiple conformational sub-states of close energy [22]. Notwithstanding the wide literature on the solution behavior of PNIPAM chains, very little is known on their properties at high concentrations and in the low-temperature regime [23].

In this Letter, we provide a comprehensive investigation of the atomic dynamics of PNIPAM linear chains at low T combining elastic incoherent neutron scattering (EINS) experiments at various energy resolutions and atomistic molecular dynamics (MD) simulations. Our results show the occurrence of a dynamical transition at $T_d \sim 225$ K, a value very similar to that observed in proteins. This result implies a wide generality of the phenomenon, independently of the structural details of the investigated complex macromolecular system.

EINS experiments were carried out at the neutron spectrometers IN16B, IN13, and IN5 [24] of Institut Laue-Langevin (ILL, Grenoble, France) [1, 2]. We mea-

* Corresponding author: emanuela.zaccarelli@cnr.it

† Corresponding author: andrea.orecchini@unipg.it

sured PNIPAM chains dispersed in D₂O at three different polymer concentrations: 50, 60 and 95 wt% (dry sample). As the neutron incoherent cross-section of hydrogen exceeds by more than one order of magnitude the total (coherent plus incoherent) cross-section of deuterium and of other atomic species in the samples, the measured signal provides information on the dynamics of polymer chains, while water contribution is negligible.

The observable quantity in an EINS experiment is the intensity $I(Q, E = 0) \equiv I(Q, 0)$ scattered in a narrow energy window centered at the elastic peak $E = 0$, as a function of exchanged momentum Q . This observable was monitored as a function of T using instruments with different energy resolution ΔE , allowing us to resolve atomic motions in a wide range of timescales τ , from ps to ns. The main characteristics of the instruments are summarized in Table I, whereas the details of experiments and data reduction are thoroughly described in the Supplemental Material [27].

	IN16B	IN13	IN5 (1 ΔE)	IN5 (2 ΔE)
Q -range (\AA^{-1})	0.2–1.9	0.2–4.5	0.55–2.0	0.55–2.0
ΔE (μeV)	0.75	8	97	191
τ (ps)	1800	150	15	7

TABLE I. Explored Q -range, energy resolution ΔE , and probed timescale τ of the used spectrometers. For IN16B and IN13 ΔE is the energy resolution (full width at half maximum), while for IN5 it is the E -window used to calculate $I(Q, 0)$. In the experimental configuration, the actual resolution of IN5 is $\Delta E \sim 87 \mu\text{eV}$, see the Supplemental Material [27].

We start by reporting the integrated elastic intensity $I_\tau(T)$, i.e. the integral over the whole measured Q -range of $I(Q, 0)$ at a given τ , as a function of temperature. Figure 1(a) shows $I_{150}(T)$ measured at IN13 for different polymer weight fractions. While the dry system displays a linear decrease of $I_{150}(T)$ with increasing T , the intensity of the two hydrated samples undergoes a clear drop at a temperature that can be located roughly within 225 K and 250 K. The departure from the linear trend marks the onset of anharmonic motions ascribed to the occurrence of the dynamical transition [1]. Within the available T -resolution, T_d does not show a dependence on sample concentration, while the extent of the drop in $I_{150}(T)$ does. Hence, for the dry sample the transition disappears, in agreement with studies suggesting a driving role of water in the transition [4, 6, 28]. These findings are in quantitative agreement with IN13 measurements on PNIPAM microgel networks [13], reported for comparison in Fig. 1(b). A nearly identical T -behavior for $I_{150}(T)$ at corresponding concentrations is observed for the two systems. Therefore, we conclude that there is no difference between cross-linked and linear chains, highlighting the fact that the dynamical transition does not depend on the details of the internal macromolecular architecture, similarly to what observed for biological

systems.

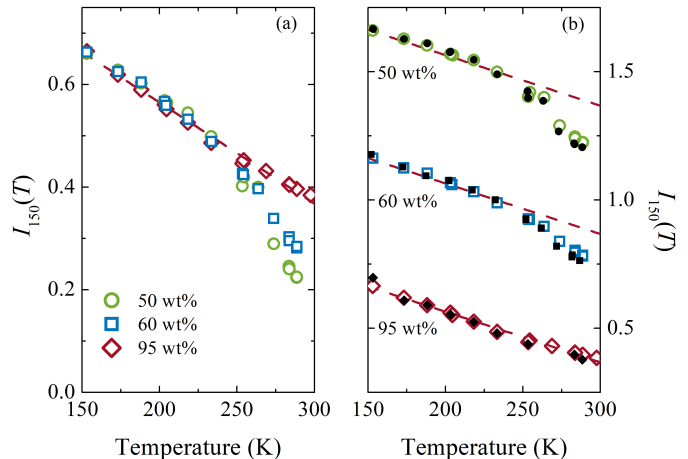


FIG. 1. IN13 integrated elastic intensity $I_{150}(T)$ as a function of temperature for (a) chains as a function of PNIPAM concentration and (b) PNIPAM chains (open symbols) compared to PNIPAM microgels (filled symbols). The dashed lines are linear fits to the data of the dry polymer chain. Data are normalized to 1 for $T \rightarrow 0$. In (b), data at different concentrations are shifted by 0.5 for clarity.

Since there is no strong dependence of T_d on wt%, from now on we focus on the 60 wt% sample only. Figure 2 shows the integrated elastic intensity $I_{1800}(T)$ measured at IN16B, which displays three different regimes: (i) a linear decrease above 150 K, that in proteins is known to account for both harmonic movements and methyl groups rotation [29, 30]; (ii) a second, steeper linear decrease above $T_d \sim 225$ K, which marks the dynamical transition; (iii) a third, sudden drop around 270 K. The latter, that is not clearly separated from (ii) on the less resolved T -scan performed on IN13, might be related to ice melting. Although there is evidence that no macroscopic crystallization takes place in the samples [13, 23], it could still be possible that a small fraction of water molecules forms a few ordered clusters, whose melting also has an echo in the polymer dynamics. Additional experiments, particularly by Differential Scanning Calorimetry, would be needed to confirm this hypothesis and to quantify the amount of residual crystalline water.

Thanks to the IN16B high flux, we acquired data using a finer temperature sampling with respect to IN13, being able to determine with great accuracy that the dynamical transition in linear chains takes place at about 225 K, well below the value of 250 K that was initially hypothesized for microgel systems [13, 14]. Given that microgels and linear chains display an identical behaviour on IN13, we expect the true T_d of microgels to be close to 225 K too.

The inset of Fig. 2 reports a comparison among all measured intensities $I_\tau(T)$ obtained by integrating $I(Q, 0)$ measured at various τ on a common Q -range. Qualitatively, data show a less and less pronounced intensity decrease as τ gets shorter, ending up in a flattening of the curve when the static approximation $\tau \rightarrow 0$ is ap-

proached. All curves at finite τ exhibit a change of slope around ~ 225 K. Hence, the present data do not suggest a clear dependence of T_d on the experimental resolution, at variance with previous reports for hydrated protein powders [31]. This discrepancy might be due to either a true difference between PNIPAM and proteins or possibly to the sparse T sampling of our IN13 and IN5 data.

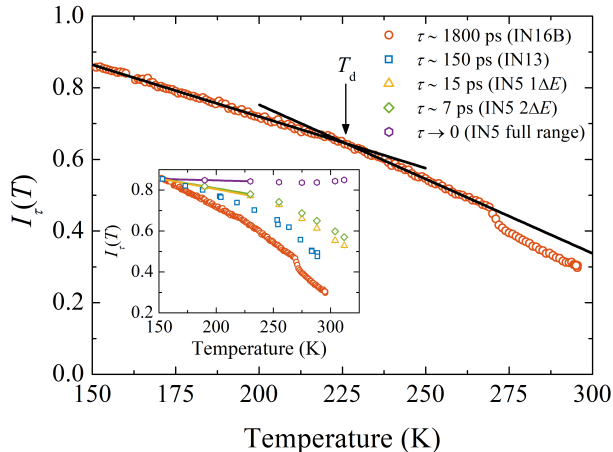


FIG. 2. IN16B integrated elastic intensity of 60 wt% linear chains. The dynamical transition temperature $T_d = 226 \pm 1$ K is determined as the crossing point of two linear behaviours (black lines). Inset: $I_\tau(T)$ obtained by integrating $I(Q, 0)$ measured at different τ in the common Q -range from 0.6 to 1.8 \AA^{-1} . IN13 data are normalized to IN16B ones at 150 K ; for IN5 ones normalization is obtained through a linear extrapolation of the lowest T -measurements (solid lines).

For a quantitative analysis of the T -evolution of polymer dynamics, we use the widely-employed double-well model for incoherent elastic scattering [1, 32], which assumes that the sample hydrogen atoms can jump between two distinct sites of different free energy separated by a distance d . Hence, $I(Q, 0)$ can be written as

$$I(Q, 0) = I_0 e^{-bQ^2} \left[1 - 2p_1 p_2 \left(1 - \frac{\sin(Qd)}{Qd} \right) \right], \quad (1)$$

where I_0 is an intensity prefactor, $b = \langle \Delta u^2 \rangle_{vib}$ is the harmonic vibrational MSD of an atom moving within a single well, p_1 and p_2 are the probabilities of finding the atom in the first or second well, respectively. For a robust determination of the physical parameters of interest, we set up a novel global analysis procedure that simultaneously fits the data acquired at all the measured timescales, over the three different Q -ranges and over all temperatures (see Supplemental Material [27]). Specifically, we assume that: (i) the harmonic behavior of our samples is faster than any of the experimental timescales τ in Tab. 1, thus being equally resolved by the three employed spectrometers; (ii) upon increasing τ , hydrogen atoms can explore a wider spatial region, hence d increases. Consequently, we constrain $\langle \Delta u^2 \rangle_{vib}$ to follow a linear behavior in T with τ -independent parameters, whereas I_0 and $p_1 p_2$ are free to vary with both τ

and T . In this way, we find that d is roughly constant in T but grows with τ as $d(\tau) = \phi \tau^\xi$, in agreement with previous findings for proteins [31]. We thus enforce d to follow such a power-law behavior with ϕ and ξ as additional fit parameters. From this model, we can finally estimate the total MSD [32] of PNIPAM hydrogen atoms for each time resolution, as

$$\text{MSD} = 6 \langle \Delta u^2 \rangle_{vib} + 2p_1 p_2 d^2. \quad (2)$$

Figure 3 reports the experimentally determined MSDs at the different time resolutions as a function of T . As expected, at a given temperature MSDs are larger for longer observation timescales τ . Considering IN16B and IN13 data, we easily recognize the same three regimes also observed for the integrated elastic intensity in Fig. 2. Our results do not show a clear evolution of T_d with τ . In proteins, the existence of this dependence is debated and results range from a strong variation of T_d [33] to a substantially τ -independent transition [31]. In our case, we find that $T_d \sim 225 \text{ K}$ seems compatible with all datasets, although the sparse T sampling of IN13 and IN5 does not allow to unambiguously determine a possible trend.

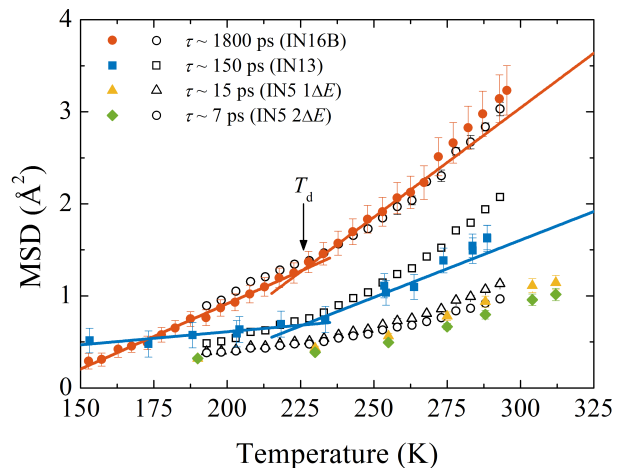


FIG. 3. Comparison between experimental MSDs (filled symbols), obtained by fitting $I(Q, 0)$ as described in the text, and numerical MSDs (open symbols) at the same timescales. When not visible, error bars are within symbol size. The transition temperature obtained from the integrated elastic intensity is marked with a black arrow. Red and blue lines highlight the transition in IN16B and IN13 data respectively.

It is now instructive to compare the experimental results with MD simulations, that were carried out on a suspension of 6 PNIPAM chains with a polymer mass fraction of 60 wt% with an explicit description of the solvent. Each chain is modelled as an atactic PNIPAM segment composed of 30 repeating units that, thanks to the covalent connectivity between adjacent periodic images, mimics the effect of the higher degree of polymerization of the chains used in the experiments [34]. PNIPAM is described with the OPLS-AA force field [9] including the implementation by Siu et al. [10], and water with the

Tip4p/ICE model [11]. Trajectory data were acquired for $0.5 \mu\text{s}$ in a wide range of temperatures, by cooling the system from 293 to 193 K. Further information is provided in the Supplemental Material [27].

The MSDs of PNIPAM hydrogen atoms directly evaluated from MD simulations at each time resolution as a function of T are also reported in Fig. 3. Remarkably, the numerical data quantitatively agree with the experimental estimates at all temperatures and for all measured time resolutions, without any arbitrary scaling factor. This confirms previous results obtained from IN13 measurements of microgels [13], crucially extending their validity by more than two decades in time. In addition, the direct comparison of experiments and simulations strongly validates the global fit procedure that we have adopted to extract experimental MSDs from the measured elastic intensities. Indeed, we stress that a free fit would not be able to provide the same level of consistency both between data measured at different E -resolution and Q -range and between experimental and numerical data. Furthermore, these findings corroborate the use of the TIP4P/ICE model, which fully captures the T -dependence of the dynamical behavior of polymer atoms, and thus emerges as the optimal water model to simulate PNIPAM dynamics in supercooled water.

The numerical MSD data substantiate the behavior of the integrated elastic intensity and also point to the occurrence of a dynamical transition for linear PNIPAM chains around $T_d \sim 225$ K. While simulations have been performed with a temperature mesh of 5 K, due to the long simulation time required for each state point, this sampling is sufficient to locate T_d in good agreement with experiments. We remark that a different value of T_d , roughly around 250 K, was previously reported for microgels [13, 14], but this larger value can be entirely ascribed to the broader T -sampling used in such earlier studies.

The use of simulations further allows us to identify the specific motions underlying the onset of the transition, which should be connected, as in proteins [38], to the activation of local segment motions. This is investigated by monitoring the fraction of mobile backbone dihedral angles x_m as a function of T , that is shown in Fig. 4a. We find that, compatibly with statistical uncertainty, x_m becomes larger than zero for $T \gtrsim 230$ K, thus confirming the molecular origin of the transition with the activation of bond flips between rotational isomeric states of the chain backbone. We stress that this analysis has been performed on the whole equilibrated run, so that its results can be considered to be independent of time resolution. Finally, it is important to note that while methyl hydrogen atoms are active at all investigated temperatures (see Supplemental Material [27]), backbone hydrogen atoms are inactive below T_d , as shown by their MSDs, reported as a function of T in Fig. 4b for different values of τ . Clearly, deviations from a low- T linear regime again occur only for temperatures higher than 225 K. These results confirm that, also in the simulation data, the value of T_d is independent of the probed time window.

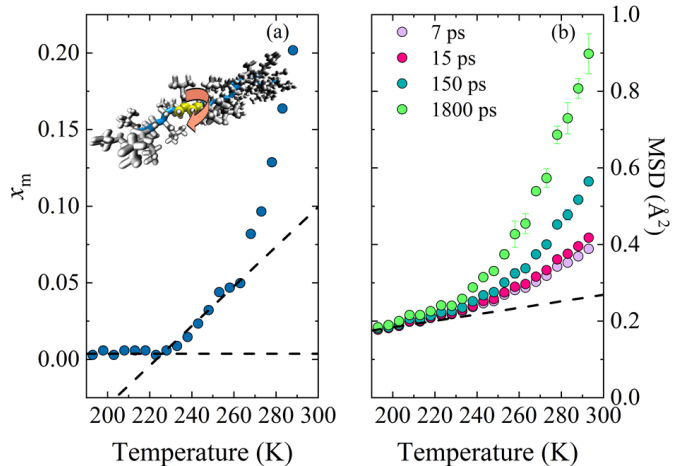


FIG. 4. MD results for a) fraction of mobile backbone dihedral angles x_m and b) MSD of hydrogen backbone atoms for different time resolutions, both as a function of temperature. A snapshot of a polymer chain is also shown in a), with backbone atoms in blue and a dihedral angle highlighted in yellow. In both panels, dashed lines are guides to the eye to indicate the occurrence of the dynamical transition at $T_d \sim 225$ K. When not visible, error bars are within symbol size.

In this work we reported evidence of a low-temperature dynamical transition in linear PNIPAM polymer chains by means of EINS measurements at resolutions covering more than two decades in time. A global fit, based on the double-well model, was simultaneously applied to all measured data as a function of T , Q and E , allowing us to extract the MSDs of PNIPAM hydrogen atoms, which were found to be in quantitative agreement with those calculated in atomistic MD simulations. Our results clearly indicate that the dynamical transition takes place at $T_d \sim 225$ K, a value remarkably close to that observed for proteins. The value of T_d seems to be independent from the experimental resolution, although further studies are needed to fully clarify this point. We thus confirm the occurrence of a dynamical transition in aqueous suspensions of non-biological systems [13, 39], further indicating that this phenomenon is not dictated by the internal polymer architecture, but emerges as a more generic process. The present findings further challenge the relation between the dynamical behavior of a macromolecule and its biological functionality and call for a deepening of the understanding of the molecular mechanisms taking place in such a transition.

ACKNOWLEDGMENTS

We acknowledge ILL for beamtime and CINECA-ISCRA for computer time. LT, MB, EC and EZ acknowledge support from European Research Council (ERC-CoG-2015, Grant No. 681597 MIMIC); LT, EB, EC and EZ

from MIUR (FARE project R16XLE2X3L, SOFTART) and from Regione Lazio, through L.R. 13/08, Progetto

Gruppo di Ricerca GELARTE n.prot.85-2017-15290. LT and MZ contributed equally to this work.

-
- [1] W. Doster, S. Cusack, and W. Petry, *Nature* **337**, 754 (1989).
- [2] M. Ferrand, A. J. Dianoux, W. Petry, and G. Zaccai, *Proc. Natl. Acad. Sci. USA* **90**, 9668 (1993).
- [3] G. Zaccai, *Science* **288**, 1604 (2000).
- [4] M. Tarek and D. J. Tobias, *Phys. Rev. Lett.* **88**, 138101 (2002).
- [5] K. Wood, A. Frölich, A. Paciaroni, M. Moulin, M. Härtlein, G. Zaccai, D. J. Tobias, and M. Weik, *J. Am. Chem. Soc.* **130**, 4586 (2008).
- [6] G. Schirò, Y. Fichou, F.-X. Gallat, K. Wood, F. Gabel, M. Moulin, M. Härtlein, M. Heyden, J.-P. Colletier, A. Orecchini, *et al.*, *Nat. Commun.* **6**, 6490 (2015).
- [7] O. Rahaman, M. Kalimeri, M. Katava, A. Paciaroni, and F. Sterpone, *J. Phys. Chem. B* **121**, 6792 (2017).
- [8] G. Schirò and M. Weik, *J. Phys.: Cond. Matt.* **31**, 463002 (2019).
- [9] Z. Liu, J. Huang, M. Tyagi, H. O'Neill, Q. Zhang, E. Mamtov, N. Jain, Y. Wang, J. Zhang, J. C. Smith, and L. Hong, *Phys. Rev. Lett.* **119**, 048101 (2017).
- [10] E. Cornicchi, S. Capponi, M. Marconi, G. Onori, and A. Paciaroni, *Phil. Mag.* **87**, 509 (2007).
- [11] G. Caliskan, R. M. Briber, D. Thirumalai, V. Garcia-Sakai, S. A. Woodson, and A. P. Sokolov, *J. Am. Chem. Soc.* **128**, 32 (2006).
- [12] J. Peters, J. Marion, F. Natali, E. Kats, and D. J. Bicout, *J. Chem. Phys. B* **121**, 6860 (2017).
- [13] M. Zanatta, L. Tavagnacco, E. Buratti, M. Bertoldo, F. Natali, E. Chiessi, A. Orecchini, and E. Zaccarelli, *Sci. Adv.* **4**, eaat5895 (2018).
- [14] L. Tavagnacco, E. Chiessi, M. Zanatta, A. Orecchini, and E. Zaccarelli, *J. Phys. Chem. Lett.* **10**, 870 (2019).
- [15] A. Fernandez-Nieves, H. Wyss, J. Mattsson, and D. A. Weitz, *Microgel suspensions: fundamentals and applications* (John Wiley & Sons, 2011).
- [16] Y. He, P. I. Ku, J. R. Knab, J. Y. Chen, and A. G. Markelz, *Phys. Rev. Lett.* **101**, 178103 (2008).
- [17] G. Schirò, C. Caronna, F. Natali, M. M. Koza, and A. Cupane, *J. Phys. Chem. Lett.* **2**, 2275 (2011).
- [18] J. Rubio Retama, B. Frick, T. Seydel, M. Stamm, A. Fernandez Barbero, and E. López Cabarcos, *Macromolecules* **41**, 4739 (2008).
- [19] M. Karg, A. Pich, T. Hellweg, T. Hoare, L. A. Lyon, J. J. Crassous, D. Suzuki, R. A. Gumerov, S. Schneider, I. I. Potemkin, *et al.*, *Langmuir* **35**, 6231 (2019).
- [20] L. Rovigatti, N. Gnan, L. Tavagnacco, A. J. Moreno, and E. Zaccarelli, *Soft matter* **15**, 1108 (2019).
- [21] S. Fujishige, K. Kubota, and I. Ando, *J. Phys. Chem.* **93**, 3311 (1989).
- [22] E. I. Tiktopulo, V. N. Uversky, V. B. Lushchik, S. I. Klenin, V. E. Bychkova, and O. B. Ptitsyn, *Macromolecules* **28**, 7519 (1995).
- [23] F. Afroze, E. Nies, and H. Berghmans, *J. Mol. Struct.* **554**, 55 (2000).
- [24] www.ill.eu/users/instruments/.
- [1] M. Zanatta, M. Bertoldo, E. Buratti, F. Natali, J. Ollivier, A. Orecchini, J. M. Ruiz Franco, L. Tavagnacco, and E. Zaccarelli, “Low-temperature dynamical transition in polymeric aqueous environments,” (2018), doi:10.5291/ILL-DATA.9-11-1866.
- [2] L. Tavagnacco, M. Bertoldo, E. Buratti, F. Camerin, B. Frick, J. Ollivier, A. Orecchini, P. Tozzi, E. Zaccarelli, and M. Zanatta, “Investigation of supercooled water dynamics by confinement in dense microgel suspensions,” (2018), doi:10.5291/ILL-DATA.9-11-1864.
- [27] See Supplemental Material for more details on the sample preparation, the neutron scattering data collection and analysis, and the simulation protocol.
- [28] G. Camisasca, M. De Marzio, D. Corradini, and P. Gallo, *J. Chem. Phys.* **145**, 044503 (2016).
- [29] J. H. Roh, V. N. Novikov, R. B. Gregory, J. E. Curtis, Z. Chowdhuri, and A. P. Sokolov, *Phys. Rev. Lett.* **95**, 038101 (2005).
- [30] G. Schirò, C. Caronna, F. Natali, and A. Cupane, *J. Am. Chem. Soc.* **132**, 1371 (2010).
- [31] G. Schirò, F. Natali, and A. Cupane, *Phys. Rev. Lett.* **109**, 128102 (2012).
- [32] M. Katava, G. Stirnemann, M. Zanatta, S. Capaccioli, M. Pachetti, K. Ngai, F. Sterpone, and A. Paciaroni, *Proc. Natl. Acad. Sci. USA* **114**, 9361 (2017).
- [33] K. L. Ngai, S. Capaccioli, and A. Paciaroni, *The Journal of Chemical Physics* **138**, 235102 (2013).
- [34] L. Tavagnacco, E. Zaccarelli, and E. Chiessi, *Phys. Chem. Chem. Phys.* **20**, 9997 (2018).
- [9] W. L. Jorgensen, D. S. Maxwell, and J. Tirado-Rives, *J. Am. Chem. Soc.* **118**, 11225 (1996).
- [10] S. W. I. Siu, K. Pluhackova, and R. A. Böckmann, *J. Chem. Theory Comput.* **8**, 1459 (2012).
- [11] J. L. F. Abascal, E. Sanz, R. G. Fernández, and C. Vega, *J. Chem. Phys.* **122**, 234511 (2005).
- [38] B. F. Rasmussen, A. M. Stock, D. Ringe, and G. A. Petsko, *Nature* **357**, 423 (1992).
- [39] A. Iorio, G. Camisasca, and P. Gallo, *J. Mol. Liq.* **282**, 617 (2019).

I. SAMPLE PREPARATION

Poly(N-isopropylacrylamide) (molecular weight $M_w = 189600$ and polydispersity index $PDI = 2.88$) was purchased from Polymer Source Inc. and used without further purification. A suspension with a polymer concentration of 10 wt% was prepared through 3 cycles of lyophilization and dispersion in D_2O . High concentration samples were then obtained by filling the holders with the dispersion at 10 wt% and then allowing the exceeding D_2O to evaporate at room temperature under vacuum. Once the desired concentration of 50 wt%, 60 wt% and 95 wt% were reached, the holders were sealed and samples were left to homogenize for not less than four days.

II. ELASTIC INCOHERENT NEUTRON SCATTERING DATA COLLECTION

EINS experiments were carried out at the neutron spectrometers IN16B, IN13, and IN5 of the Institut Laue-Langevin (ILL, Grenoble, France) [S1, S2]. The samples were measured inside flat aluminium cells (3.0×4.0 cm) sealed with an In o-ring. The thickness of each cell was selected to achieve a transmission of about 90% considering an incoming wavelength $\lambda_i = 6.271$ Å. The weight of each sample was checked before and after each measurement without observing any appreciable variation.

A. IN13 data

IN13 is a high-resolution backscattering spectrometer using thermal neutrons. In the elastic configuration, IN13 operates with an incident wavelength $\lambda_i = 2.23$ Å and covers an interval of exchanged momentum Q from about 0.2 to 4.5 Å⁻¹ with an energy resolution is $\Delta E = 8$ μeV (FWHM). Measurements were carried out on the 50, 60, and 95 wt% PNIPAM linear chain samples. The $I(Q, 0)$ was acquired at selected fixed temperatures, cooling the sample from about 290 K down to 150 K and then heating it to room temperature again. The acquisition time for each temperature ranged from 30 minutes up to 2 hours.

Data were normalized to take into account for incident flux, cell scattering and self-shielding. The $I(Q, 0)$ of each sample was normalized to a vanadium standard to account for detector efficiency fluctuations. Multiple scattering processes were neglected. Figure S1 shows the so-obtained $I(Q, 0)$ for the three samples.

B. IN16B data

Measurements at the high-flux backscattering spectrometer IN16B were done in the Si (111) configuration, which allows an elastic E -resolution of $\Delta E = 0.75$ μeV (FWHM) using neutrons with an incident wavelength $\lambda_i = 6.271$ Å. Data are acquired over a Q -range from about 0.2 to 1.9 Å⁻¹. The $I(Q, 0)$ were measured on the 60 wt% sample during a heating ramp with a controlled heating rate of 0.3 K/min. The acquisition time was 30 s for each $I(Q, 0)$.

Data were normalized to take into account for incident flux, cell scattering and self-shielding. Each $I(Q, 0)$ was normalized to a low-temperature measurement of the sample. Multiple scattering processes were neglected. Figure S2 shows the so obtained T -evolution of the $I(Q, 0)$ for the 60 wt% PNIPAM linear chains sample.

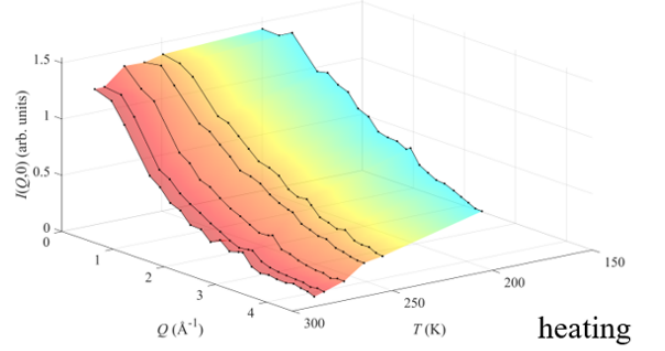
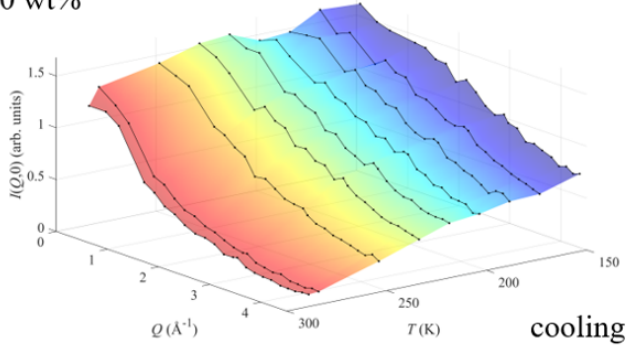
C. IN5 data

The time-of-flight (ToF) spectrometer IN5 allows measuring the full dynamic structure factor $S(Q, E)$ over a broad interval of the exchanged energy E and momentum Q . The instrument was configured to select neutrons with incident wavelength $\lambda_i = 5$ Å with a chopper speed of 12000 rpm. This ensures an energy resolution $\Delta E = 87$ μeV (FWHM). The energy resolution was obtained by fitting the elastic peak measured on a Vanadium sample with a Gaussian function. Measurements were carried out on the 60 wt% sample. Data were acquired at selected fixed temperatures, heating the sample from about 190 K up to 312 K. The acquisition time for each temperature was 1 hour.

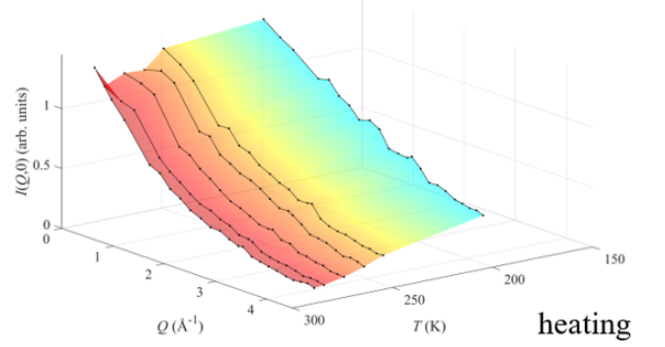
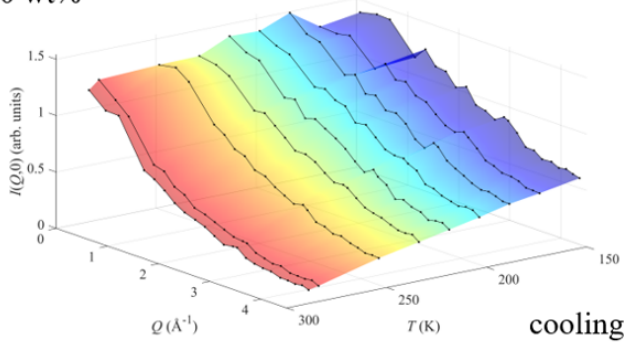
A proper data reduction was done to take into account for incident flux, cell scattering and self-shielding. Data were thus normalized to a vanadium sample and ToF spectra recorded for each scattering angle 2θ were converted into $I(2\theta, E)$ ones. Multiple scattering processes were neglected.

In order to calculate the $I(Q, 0)$, the so obtained $I(2\theta, E)$ was integrated over symmetrical regions across the elastic peak with extension $1\Delta E = 97$ μeV and $2\Delta E = 191$ μeV. Finally, the scattering angle 2θ was transformed into an

50 wt%



60 wt%



95 wt%

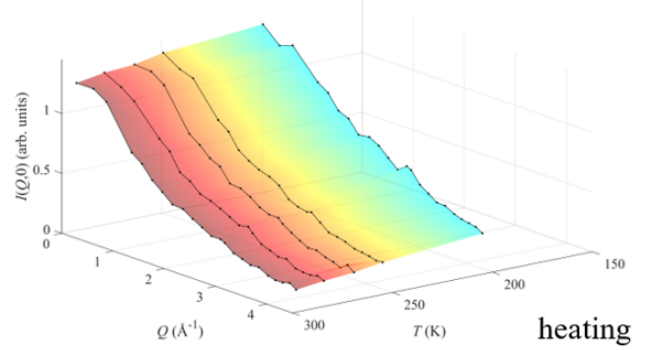
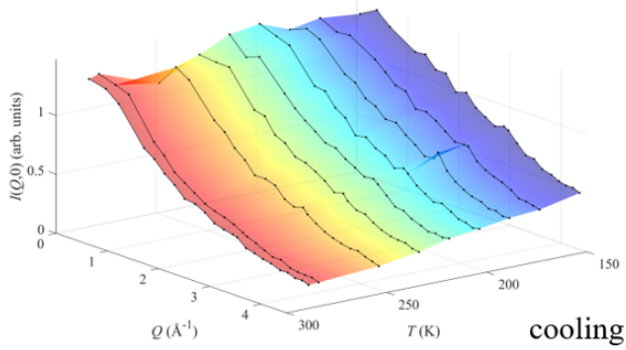


FIG. S1. Temperature evolution of the elastic incoherent intensity $I(Q,0)$ measured at IN13 for the three samples during the cooling cycle (left panels) and the heating one (right panels).

elastic Q . This leads to an $I(Q,0)$ in a Q -range between 0.55 and 2.0 \AA , while below 0.55 \AA , the $I(Q,0)$ shows an unphysical behaviour, probably due to a problem in the vanadium normalization. Figure S3 shows the results.

III. ELASTIC INCOHERENT NEUTRON SCATTERING DATA ANALYSIS

As thoroughly described in the manuscript, EINS data were fitted using the double-well model [S3, S4]. Here we recall only the expression for the $I(Q,0)$,

$$I(Q,0) = I_0 e^{-bQ^2} \left[1 - 2p_1 p_2 \left(1 - \frac{\sin(Qd)}{Qd} \right) \right], \quad (\text{S3})$$

where I_0 is an intensity prefactor, $b = \langle \Delta u^2 \rangle_{vib}$ is the harmonic vibrational MSD of an atom moving within a single well, p_1 and p_2 are the probabilities of finding the atom in the first or second well, respectively.

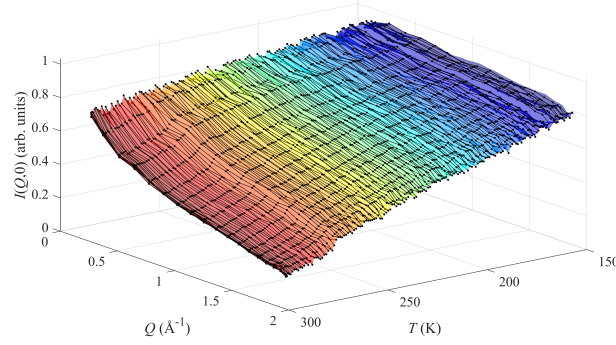


FIG. S2. Temperature evolution of the elastic incoherent intensity $I(Q, 0)$ for the 60 wt% linear chains sample as obtained from IN16B data.

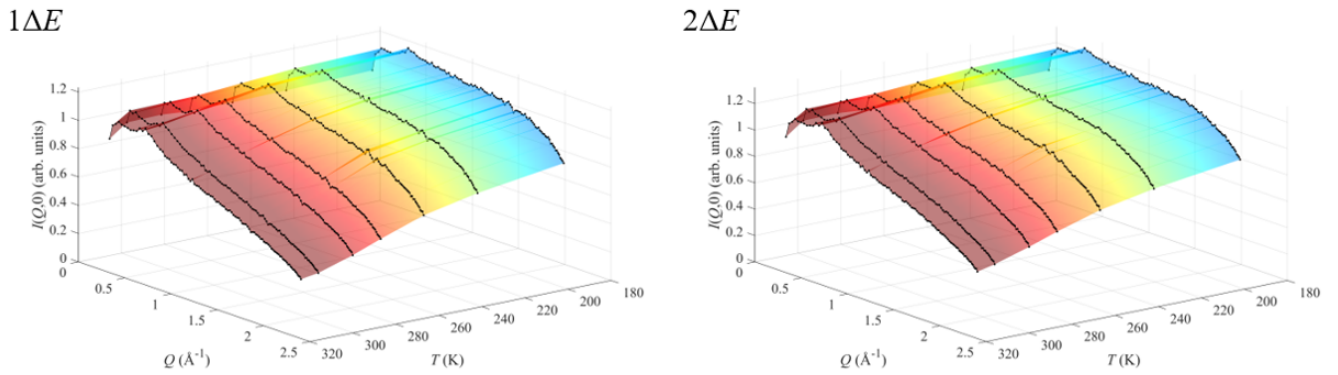


FIG. S3. Temperature evolution of the elastic incoherent intensity $I(Q, 0)$ for the 60 wt% linear chains sample as obtained from IN5 data integrated over $1\Delta E$ (left panel) and $2\Delta E$ (right panel).

The data acquired at the three different energy resolutions, over the three different Q -ranges and over all temperatures were fitted simultaneously within a global fit procedure. To do so, we assumed that:

- I_0 depends both on τ and T so it is a *local* parameter for each $I(Q, 0)$;
- b does not depend on τ , while following a linear dependence on T , then $b(T) = q + mT$ with q and m *global* parameters common to all the datasets;
- p_1 and p_2 depend both on τ and T so they are *local* parameters for each $I(Q, 0)$;
- d does not depend on T ;
- the dependence of d on τ can be written as a power law of the form $d = \phi\tau^\xi$ [S5], where ϕ is related to the diffusion coefficient, while the exponent $\xi < 0.5$ takes into account a possible subdiffusive behaviour often observed in polymeric systems [S6].

Results for the 60 wt% sample are shown in Figs. S4 S5 S6. Within this approach, the model describes very well our data providing also a good agreement with the simulations, see Fig. 3 in the manuscript.

To improve the signal to noise ratio, the $I(Q, 0)$ acquired on IN16B were binned over T -channels of 5 K. The temperature of the final data is the average temperature of the $I(Q, 0)$ inside each T -channel.

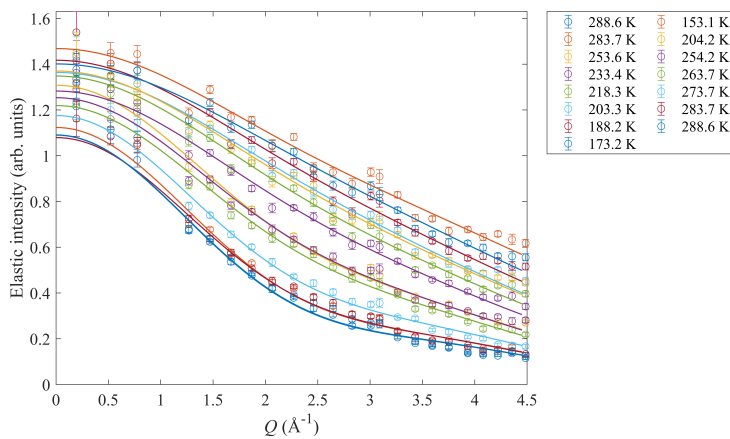


FIG. S4. Typical fits of the $I(Q,0)$ measured on IN13 in PNIPAM linear chains at 60 wt%. Colors are as in the legend.

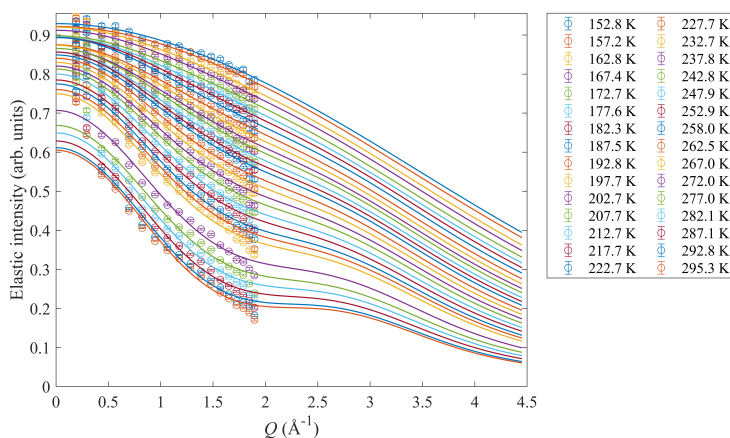


FIG. S5. Typical fits of the $I(Q,0)$ measured on IN16B in PNIPAM linear chains at 60 wt%. Colors are as in the legend.

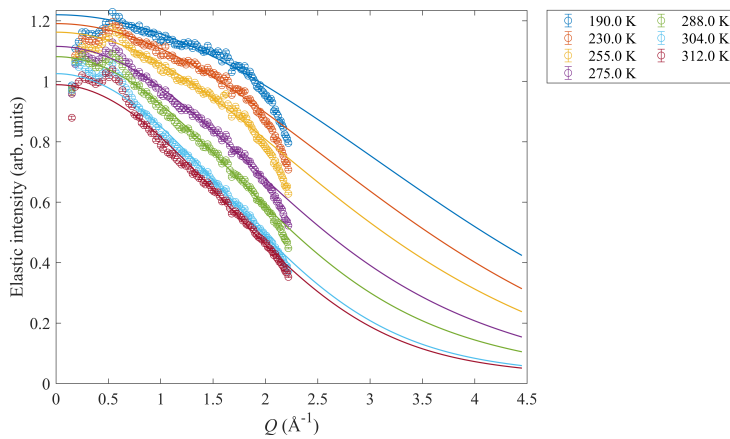


FIG. S6. Typical fits of the $I(Q,0)$ measured on IN5 in PNIPAM linear chains at 60 wt%. Colors are as in the legend.

IV. MOLECULAR DYNAMICS SIMULATIONS PROCEDURE

The *in silico* model of PNIPAM linear chains suspension in water was designed by including in a cubic box 6 polymer segments made of 30 repeating units, with an extra-boundary connectivity between adjacent periodic images to mimic the effect of the higher degree of polymerization in the experimental samples, and by adding explicit water. A schematic representation of the model is shown in Fig. S7. All-atom MD simulations were performed on linear polymer chains suspensions with PNIPAM mass fraction of 60% using the GROMACS 5.1.4 software [S7, S8]. PNIPAM and water were described using the OPLS-AA force field [S9] with the implementation by Siu et al. [S10] and the Tip4p/ICE model [S11], respectively. Numerical simulations were carried out in a range of temperature between 293 K and 193 K, with a temperature step of 5 K, due to the long simulation time required for each state point. Indeed, at each temperature the system was first equilibrated in a pressure bath at 1 bar, maintained by the Parrinello–Rahman barostat with a time constant of 2 ps, up to a constant density value, i.e. tot-drift less than $2 \times 10^{-3} \text{ g cm}^{-3}$ over 20 ns. Simulation data were then collected for 330 ns in the NVT ensemble, with a sampling of 0.2 frame/ps. The leapfrog integration algorithm was employed with a time step of 2 fs. The length of bonds involving hydrogen atoms was kept fixed with the LINCS algorithm. Cubic periodic boundary conditions and minimum image convention were applied. The temperature was controlled with the velocity rescaling thermostat [S12] with a time constant of 0.1 ps. Electrostatic interactions were treated with the smooth particle-mesh Ewald method with a cutoff of non-bonded interactions of 1 nm. A total trajectory interval of about $0.5 \mu\text{s}$ was calculated for each temperature. The last 300 ns of trajectory were considered for analysis. The software VMD [S13] was employed for graphical visualization.

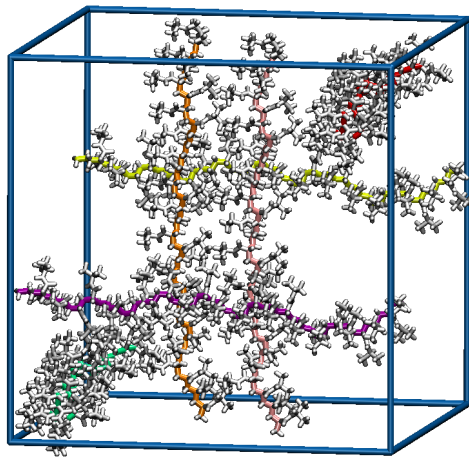


FIG. S7. Schematic representation of the atomistic model of PNIPAM chains suspension in water prior to density equilibration. Backbone carbon atoms of each polymer chain are represented with a different colour, while hydrogen atoms and heavy atoms in the side chains groups are displayed in gray. Water molecules are omitted for clarity.

V. PNIPAM INTERNAL DYNAMICS FROM MOLECULAR DYNAMICS SIMULATIONS

We investigate the onset of anharmonic motions in the polymer chains by monitoring the conformation and torsional dynamics of dihedral angles. In the analysis of the torsional dynamics of methyl groups in PNIPAM side chains, we defined the dihedral of the methyl group as the angle formed by the atoms $N - C_{isopropyl} - C_{methyl} - H$, whereas for backbone dihedral angles we considered four consecutive backbone carbon atoms. As shown in Table S2, transitions between conformational states of methyl groups are observed at each temperature and all the dihedrals angles are active in the whole temperature range. On the contrary, in the case of backbone dihedral angles, a clear increase of the number of mobile dihedral angles occurs at T_d .

We quantitatively compared the experimental and numerical results by calculating the numerical mean squared displacement of PNIPAM hydrogen atoms, MSD , from the following equation:

$$MSD(t) = \langle |r_H(t) - r_H(0)|^2 \rangle \quad (\text{S4})$$

where $r_H(t)$ and $r_H(0)$ are the position vectors of a PNIPAM hydrogen atom at time t and 0, averaged over time origins and hydrogen atoms.

TABLE S2. Torsional dynamics of the polymer dihedral angles

x_m			x_m		
T (K)	Backbone	Methylgroups	T (K)	Backbone	Methylgroups
193	0.29	100	243	2.3	100
198	0.58	100	248	3.2	100
203	0.29	100	253	4.4	100
208	0.58	100	258	4.7	100
213	0.58	100	263	5.0	100
218	0.58	100	268	8.2	100
223	0.29	100	273	9.6	100
228	0.58	100	278	13	100
233	0.88	100	283	16	100
238	1.5	100	288	20	100

T is the temperature and x_m is the percentage of mobile dihedrals. Analysis over the last 300 ns.

In addition to the MSDs of all PNIPAM hydrogen atoms and those in the backbone, we have also calculated the contribution of the MSDs of the hydrogen atoms in the methyl groups which also exhibits a change at $T_d \sim 225$ K (Fig. S8).

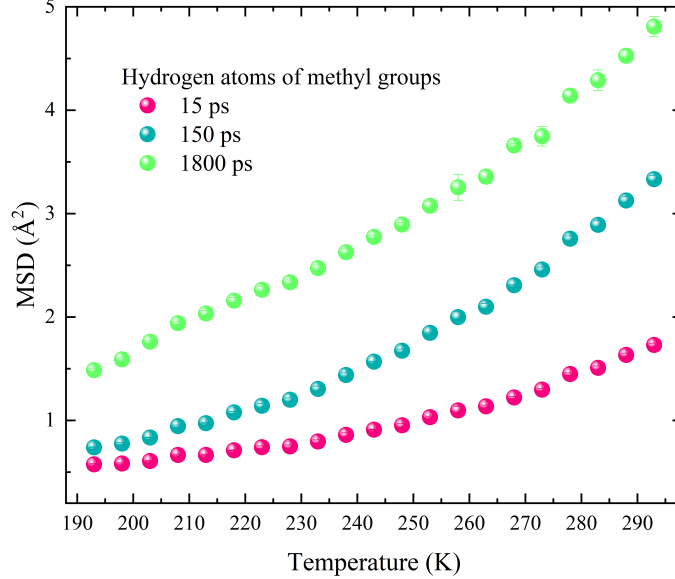


FIG. S8. Temperature dependence of MSDs of hydrogen atoms belonging to the methyl groups calculated at different time resolution: 15 ps (pink), 150 ps (blue) and 1800 ps (green). When not visible, error bars are within symbol size.

Finally, to evaluate the role of the molecular architecture on the polymer local dynamics, we have reported in Fig. S9 a comparison between the temperature dependence of the MSDs of PNIPAM hydrogen atoms of linear chains and microgels network, whose data were taken from Ref. [S14]. Figure S9 shows a quantitative agreement between the MSDs calculated at 150 ps with no differences between the two polymer architectures.

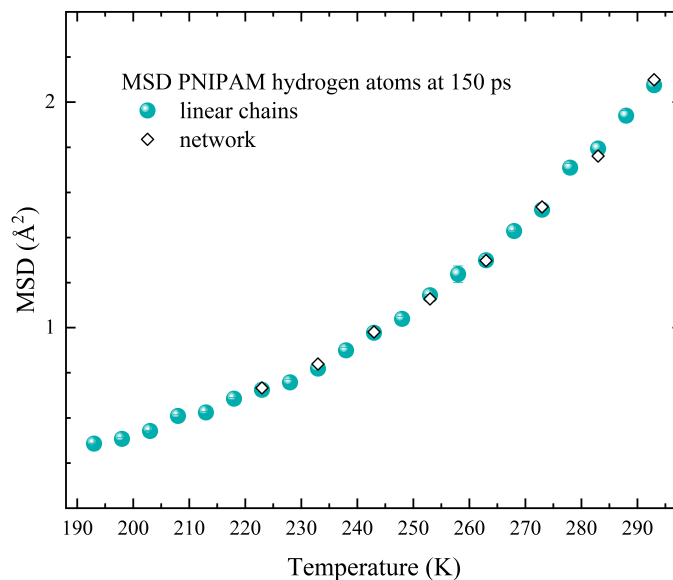


FIG. S9. Comparison between the temperature dependence of PNIPAM hydrogen atoms MSDs calculated from MD simulations at 150 ps at a concentration of 60 wt% of linear polymer chains (blue circles) or polymer network (white diamonds) [S14]. When not visible, error bars are within symbol size.

-
- [S1] M. Zanatta *et al.*, Low-temperature dynamical transition in polymeric aqueous environments, doi:10.5291/ILL-DATA.9-11-1866 (2018).
- [S2] L. Tavagnacco *et al.*, Investigation of supercooled water dynamics by confinement in dense microgel suspensions, doi:10.5291/ILL-DATA.9-11-1864 (2018).
- [S3] W. Doster, S. Cusack, and W. Petry, Dynamical transition of myoglobin revealed by inelastic neutron scattering, *Nature* **337**, 754 (1989).
- [S4] M. Katava, G. Stirnemann, M. Zanatta, S. Capaccioli, M. Pachetti, K.L. Ngai, F. Sterpone, and A. Paciaroni, Critical structural fluctuations of proteins upon thermal unfolding challenge the Lindemann criterion, *Proc. Natl. Acad. Sci. USA* **114**, 9361-9366 (2017).
- [S5] G. Schirò, F. Natali, and A. Cupane, Physical origin of anharmonic dynamics in proteins: new insights from resolution-dependent neutron scattering on homomeric polypeptides, *Phys. Rev. Lett.* **109**, 128102 (2012).
- [S6] H.W. Weber and R. Kimmich, Anomalous segment diffusion in polymers and NMR relaxation spectroscopy, *Macromolecules* **26**, 2597-2606 (1993).
- [S7] S. Páll *et al.*, *Tackling Exascale Software Challenges in Molecular Dynamics Simulations with GROMACS*, (Springer International Publishing, Cham, 2015), pp. 3-27.
- [S8] M. J. Abraham, T. Murtola, R. Schulz, S. Páll, J. C. Smith, B. Hess, E. Lindahl, GROMACS: High performance molecular simulations through multi-level parallelism from laptops to supercomputers, *SoftwareX* **1–2**, 19–25 (2015).
- [S9] W. L. Jorgensen, D. S. Maxwell, J. Tirado-Rives, Development and testing of the opls all-atom force field on conformational energetics and properties of organic liquids, *J. Am. Chem. Soc.* **118**, 11225-11236 (1996).
- [S10] S. W. I. Siu, K. Pluhackova, R. A. Böckmann, Optimization of the opls-aa force field for long hydrocarbons, *J. Chem. Theory Comput.* **8**, 1459-1470 (2012).
- [S11] J. L. F. Abascal, E. Sanz, R. G. Fernández, C. Vega, A potential model for the study of ices and amorphous water: Tip4p/ice, *J. Chem. Phys.* **122**, 234511 (2005).
- [S12] G. Bussi, D. Donadio, M. Parrinello, Canonical sampling through velocity rescaling, *J. Chem. Phys.* **126**, 014101 (2007).
- [S13] W. Humphrey, A. Dalke, K. Schulten, Vmd: Visual molecular dynamics, *J. Mol. Graph.* **14**, 33–38 (1996).
- [S14] L. Tavagnacco, E. Chiessi, M. Zanatta, A. Orecchini, E. Zaccarelli, Water–polymer coupling induces a dynamical transition in microgels, *J. Phys. Chem. Lett.* **10**, 870-876 (2019).